Published in final edited form as:
J Am Soc Mass Spectrom. 2008 September ; 19(9): 1286–1295. doi:10.1016/j.jasms.2008.05.008.

Optimum Waveforms for Differential Ion Mobility Spectrometry (FAIMS)

Alexandre A. Shvartsburg and **Richard D. Smith**
Biological Sciences Division, Pacific Northwest National Laboratory, P.O. Box 999, Richland WA 99352

Abstract

Differential mobility spectrometry or field asymmetric waveform ion mobility spectrometry (FAIMS) is a new tool for separation and identification of gas-phase ions, particularly in conjunction with mass-spectrometry. In FAIMS, ions are filtered by the difference between mobilities in gases (K) at high and low electric field intensity (E) using asymmetric waveforms. An infinite number of possible waveform profiles make maximizing the performance within engineering constraints a major issue for FAIMS technology refinement. Earlier optimizations assumed the non-constant component of mobility to scale as E^2, producing the same result for all ions. Here we show that the optimum profiles are defined by the full series expansion of $K(E)$ that includes terms beyond the 1st that is proportional to E^2. For many ion/gas pairs, the first two terms have different signs, and the optimum profiles at sufficiently high E in FAIMS may differ substantially from those previously reported, improving the resolving power by up to 2.2 times. This situation arises for some ions in all FAIMS systems, but becomes more common in recent miniaturized devices that employ higher E. With realistic $K(E)$ dependences, the maximum waveform amplitude is not necessarily optimum and reducing it by up to ~20 – 30% is beneficial in some cases. The present findings are particularly relevant to targeted analyses where separation depends on the difference between $K(E)$ functions for specific ions.

Introduction

Differential ion mobility spectrometry (DMS) is becoming a powerful method of broad utility for analysis of gas-phase ions and separation of their mixtures.[1–5] The introduction of commercial DMS instruments and particularly their integration with mass spectrometry (MS) and/or liquid or gas chromatography since 2003 has enabled rapid growth of the number and diversity of applications that include environmental analyses,[6,7] food and water quality assurance,[8–10] bacterial typing,[11,12] forensic investigations,[13] proteomics and metabolomics,[14–17] pharmaceutical studies,[18–20] and protein folding research.[21–25] Since its earliest days, DMS has been employed to detect explosives, drugs, and chemical warfare agents, and its role in defense, security, and law enforcement settings continues expanding.[26–31]

As captured in the name, DMS separates ions based on the difference between their mobilities (K) at high and relatively low electric field intensity (E).[1,5] The mobility of any ion depends on E and the gas number density (N), and we can expand $K(E/N)$ in a series:[7,30,32,33]

$$K(E/N)=K(0)[\,1+a(E/N)]=K(0)\,[\,1+\sum_{n=1}^{\infty}a_n(E/N)^{2n}\,] \quad (1)$$

where a is the relative deviation of K from its low-field limit $K(0)$. The a_n coefficients are functions of the ion - gas molecule potential[32] and can produce $a>0$ or $a<0$, depending on

their values and E/N. In principle, one can deduce a for any ion from measurements of K at different E/N using drift tube ion mobility spectrometry (DT IMS).[32,34–36] However, that approach does not permit separating ion mixtures based on the difference, and thus is of limited analytical utility. Also, for larger polyatomic and biomolecular ions that are of most interest, the $a(E/N)$ dependence is usually weak. For E/N allowed by the electrical breakdown limitations of gases at standard temperature and pressure (STP), typical $|a|$ are ~10^{-2} (except for the smallest ions).[37] That is close to the accuracy of existing DT IMS systems, and $K(E/N)$ for sizable ions such as peptides appear flat.[38]

In DMS, $a(E/N)$ is elicited directly using a periodic time-dependent electric field $E(t)$ that comprises short segments $E_+(t)$ with high E and longer segments $E_-(t)$ with lower E of opposite polarity such that mean E over the period t_c is null (the zero-offset condition):[33,39–43]

$$\overline{E}=\frac{1}{t_c}\int_0^{t_c}E(t)dt=0 \tag{2}$$

but absolute $\overline{E}_+(t)$ and $\overline{E}_-(t$ differ. It is convenient to normalize $E(t)$ as

$$E(t)=E_D F(t) \tag{3}$$

where E_D is the peak absolute amplitude ("dispersion field") and $F(t)$ defines the functional form. The condition of $F(t)$ asymmetry is:

$$\langle F_{2n+1}\rangle = \frac{1}{t_c}\int_0^{t_c}F^{2n+1}(t)dt \neq 0 \tag{4}$$

for at least one $n \geq 1$. In earlier treatises,[33,39–43] this inequality was stipulated for $n = 1$ or all $n \geq 1$. Either condition is sufficient though not necessary, as expression (4) may equal 0 for $n = 1$ but not some greater n. Current DMS methods mainly utilize $n = 1$, but higher-order separations based on $n \geq 2$ are feasible.[44] The quantity $\langle F_3\rangle$ characterizing the waveform is known as the "form-factor",[45] $\langle F_{2n+1}\rangle$ and may be viewed as form-factors of various orders.

The asymmetry of $E(t)$ gave raise to the other name for DMS - field asymmetric waveform IMS or FAIMS. Ions with $a = 0$ would oscillate in such field without separation. In reality, the displacements during $E_+(t)$ and $E_-(t)$ do not cancel fully: ions drift in the direction of $E_+(t)$ segment when a(high E) > a(low E) and $E_-(t)$ otherwise. The net displacement over the cycle is:

$$d=\int_0^{t_c}K(E/N)E(t)dt \tag{5}$$

To employ this mechanism for spatial dispersion of ions based on $a(E/N)$, one needs a field of >~60 Td (or ~15 kV/cm at STP) over large distances. That being impractical, FAIMS is implemented as a filtering method using a constant weak "compensation field" E_C superposed on $E(t)$. A certain E_C of approximately:

$$E_C=d/(Kt_c) \tag{6}$$

offsets the net drift due to $E(t)$ for a particular species, while others with different $a(E/N)$ still migrate along the E_C axis. The $\{E(t) + E_C\}$ field is maintained in a gap between two electrodes carrying rf and dc voltages. This allows the species with correct E_C to stay balanced and pass the gap to be detected, while others move toward an electrode and are neutralized. As with other filtering techniques, such as quadrupole MS, one can fix E_C to monitor selected ions or scan E_C to reveal the spectrum of species present.

Numerous asymmetric $F(t)$ comply with eq (2); one comprises two rectangles:[33,39,40,45,46]

$$F=1 \text{ for } t=[0;t_c/(f+1)[\,;\, F=-1/f \text{ for } t=[t_c/(f+1);t_c[\tag{7}$$

where $f>1$ (Fig. 1 a, Fig. 2). The number of possible $F(t)$ is infinite even within eq (7), but not limited to it. For example, two right non-isosceles triangles (Fig. 1 b) would do. As the integral of a sum equals the sum of integrals, any sequence of $F(t)$ satisfying eqs (2, 5) that remains asymmetric will also work, e.g., a trapezoidal (Fig. 1 c) built from rectangles and triangles.

To find the best $F(t)$ for FAIMS analyses, we need to define the optimization criterion. In general, the electric field in FAIMS may not just separate different ions but also focus them to the gap median, reducing losses to electrodes.[5,46] Focusing requires inhomogeneous field created in gaps of curved (e.g., cylindrical or spherical) shape. In planar geometries, homogeneous field permits no focusing. While focusing improves ion transmission through FAIMS, it introduces discrimination based on $a(E/N)$ and limits the resolving power R by rendering ions with multiple E_C stable in the gap. For low ion currents, the disadvantages outweigh gains and the overall performance (quantified via the resolution/sensitivity diagrams) maximizes for planar gaps.[4] This study formally addresses planar FAIMS, but the conclusions should extend to all geometries. In the absence of focusing, the electric field effects separation only and the $F(t)$ providing best separation is optimum. In global analyses, that means the maximum of R normally defined as the absolute separation parameter (here E_C) divided by the full peak width at half maximum, $w_{1/2}$:

$$R=\left|E_c\right|/w_{1/2} \tag{8}$$

In targeted analyses, the resolution of specific features (e.g., X and Y) is characterized by

$$r=2\left[\left|E_c(X)-E_c(Y)\right|\right]/\left[w_{1/2}(X)+w_{1/2}(Y)\right] \tag{9}$$

This metric may be extended to three or more species.

Previous efforts to optimize FAIMS waveforms[33,39,40,45] sought to maximize $|E_C|$ rather than R, i.e., a constant $w_{1/2}$ was implied. While the choice of $F(t)$ affects the average E/N in FAIMS, and thus the average diffusion that determines the peak width,[32,47] the effect on E_C is much stronger and fixing $w_{1/2}$ is a fair approximation that we follow in this work. By eqs (5, 6), maximizing $|E_C|$ means maximizing $|d|$. Introducing the reduced mobility $K_0 = KN/N_0$ (where N_0 is N at STP) and combining eqs (1 – 5), one obtains:

$$d=K_0(0)(E_D/N)t_c\sum_{n=1}^{\infty}a_n(E_D/N)^{2n}\langle F_{2n+1}\rangle \tag{10}$$

For any a_n set, d depends on the $\langle F_{2n+1}\rangle$ values for specific $F(t)$.

Earlier $F(t)$ optimizations[33,39,40,45] have represented $a(E/N)$ by the leading ($n = 1$) term of eq (1) that commonly dominates the separation in "full-size" FAIMS systems[5] operated at E/N <~100 Td. However, terms with $n \geq 2$ are often important even here and grow quickly at higher E/N, becoming dominant at >120 Td employed in latest miniaturized[3,7,48] and reduced-pressure[49] FAIMS devices. Also, the $E(t)$ profiles were optimized for *fixed* peak (E_D) or peak-to-peak ($E_{P\text{-}P}$) amplitude, implying the maximum possible amplitude to be best. Here we show that *lowering* E_D or $E_{P\text{-}P}$ may improve separation, hence both the waveform profile and amplitude must be optimized. This is done here for realistic $a(E/N)$ functions.

Global Waveform Optimization

The rectangular $F(t)$ by eq (7) is called "ideal" as it maximizes $|d|$ and thus FAIMS resolution. This happens because E in $E_+(t)$ and $E_-(t)$ is fixed, while other forms comprise a range of E in either or both and hence are less asymmetric. Then:

$$\langle F_{2n+1} \rangle = (1 - f^{-2n})/(f+1) \tag{11}$$

All $\langle F_{2n+1} \rangle$ by eq (11) and thus d by eq (10) are trivially null for $f = 1$ when $F(t)$ is symmetric $f \Rightarrow \infty$ and when $F = 0$. Hence $|d|$ reaches maximum (d_{max}) at an intermediate f, with the optimum (f_{opt}) depending on E_D/N and relative a_n values. For the leading term of eq (10):

$$\langle F_3 \rangle = (f - 1)/f^2, \tag{12}$$

that reaches the maximum absolute $\langle F_3 \rangle$, or $\langle F_3 \rangle_{max}$, of 1/4 at[36] $f_{opt} = 2$. The maximum is not abrupt, particularly on the high-f side: e.g., the $\langle F_3 \rangle$ value is below $\langle F_3 \rangle_{max}$ by ≈11% at $f = 1.5$ or $f = 3$ and 25% at $f = 4$ (Fig. 3 a). This allows other effects to greatly shift f_{opt}, as discussed below.

This optimization assumed constant E_D, which is often limited by the electrical breakdown threshold. The optimum for rectangular $E(t)$ with fixed peak-to-peak amplitude ($E_{P\text{-}P}$), that often results from engineering limitations, differs because shifting f above 2 increases E_D (Fig. 2), and $|d|$ initially rises despite decreasing for constant E_D and $f_{opt} > 2$. Indeed:

$$E_D = f E_{P\text{-}P}/(f+1) \tag{13}$$

and eq (10) converts to:

$$d = \frac{K_0(0) f t_c}{(f+1)^2} \frac{E_{P\text{-}P}}{N} \sum_n a_n \left(\frac{E_{P\text{-}P}}{N} \right)^{2n} \frac{f^{2n} - 1}{(f+1)^{2n}} \tag{14}$$

The leading term of eq (14) is:

$$d = K_0(0) a_1 t_c \frac{f(f-1)}{(f+1)^3} \left(\frac{E_{P\text{-}P}}{N} \right)^3 \tag{15}$$

and $|d|$ has an (also gradual) maximum[40] at $f = 2 + \sqrt{3} \cong 3.73$ Fig. 3 b) when

$$d_{max}=K_0(0)\,|a_1|\,t_c\,\sqrt{3}(E_{P-P}/N)^3/18 \tag{16}$$

The trends of eq (12) and eq (15) were verified by measurements,[40,50] producing f_{opt} ~2 with constant E_D and ~3.7 with constant E_{PP}. Constraints on both $E_{P\text{-}P}$ and E_D lead to $2< f_{opt} <3.73$.

However, accepting $f = 2$ or 3.73 as the optima[33,39,40,45,51] for rectangular $F(t)$ is inaccurate because the $\langle F_{2n+1}\rangle$ quantities for $n >1$ are not null and maximize at different f (Fig. 3 a, b; Table 1). With E_D constraint, f_{opt} decreases for higher n because the $2n$ power over E_D magnifies the dissimilarity between $F_+(t)$ and $F_-(t)$, and the same ion motion disbalance requires a smaller difference in E. With the $E_{P\text{-}P}$ constraint, f_{opt} increases for higher n. So $|d|$ always maximizes at $f \neq 2$ or 3.73, unless at very low E_D/N (or for ions with unusually small a_n for $n >1$) where terms with $n >1$ are negligible. As good FAIMS separations require substantial E_D/N, the terms with $n = 2$ are usually important and those with $n = 3$ and even 4 may also be significant.[44,52] The present discussion is limited to $n \leq 2$, which often suffices[52] at moderate E_D/N (< ~80 – 100 Td).

The differences between f_{opt} values at $n = 1 – 4$, especially 1 and 2, are modest compared to the breadth of maxima of $\langle F_{2n+1}\rangle(f)$ curves (Fig. 3 a, b). Hence $\langle F_{2n+1}\rangle$ values for one n are close to their maxima at f_{opt} for other n. For example, in Fig. 3 a, the value of $\langle F_5\rangle$ at $f = 2$ is ~96% of $\langle F_5\rangle_{max}$ found at $f = 1.65$. However, the terms with $n >1$ matter for optimum $F(t)$ because $|d|$ may maximize outside of the range between f_{opt} for specific n when the signs of at least two a_n differ. With only two n (e.g., 1 and 2), this happens when a_n have opposite signs. In such cases, f_{opt} may greatly differ from that for $n = 1$ when the ratio of $n = 2$ and $n = 1$ terms in eq (1),

$$a_R=a_2(E_D/(N)^2/a_1 \tag{17}$$

is not far from −1. For instance, at $a_R = −0.8$ (with E_D constraint), d_{max} is located at f ~1.24 while at $f = 2$ we find $d = 0$, i.e., no separation occurs (Fig. 3 c)! This extreme example clearly shows that $n >1$ terms are crucial for waveform optimization when a_1 and a_2 have opposite signs, a common situation as discussed below. For further analysis, we parse eq (10) and eq (14) as

$$d=K_0(0)a_1(E_D/N)^3t_c\,\langle F\rangle=K_0(0)a_1(E_{P-P}/N)^3t_cf^3\,\langle F\rangle/(f+1)^3 \tag{18}$$

where $\langle F\rangle$ is the "effective form-factor":

$$\langle F\rangle=\langle F_3\rangle+a_R\,\langle F_5\rangle \tag{19}$$

As the separation power depends on $|E_C|$ and $|d|$, what matters is absolute $\langle F\rangle$.

First, we optimize f for constant E_D. When a_1 and a_2 have same signs, f_{opt} shifts from 2 for $n = 1$ to ≅1.65 for $n = 2$ as a_R increases (Fig. 3 c); as shown above, $f = 2$ is only slightly suboptimum even at highest a_R. With opposite a_1 and a_2 signs, f_{opt} rapidly rises with decreasing a_R (Fig. 3 c) and keeping $f = 2$ can drastically decrease absolute $\langle F\rangle$. For $a_R <−0.5$, a region of $\langle F\rangle <0$ appears at f near 1.0. As a_R decreases, the minimum moves to higher f and deepens while the maximum lowers, and for $a_R \cong −0.75$ the value of $|\langle F\rangle|$ in the minimum (at $f \cong 1.21$) reaches that in the maximum (at $f \cong 3.59$). Then the maximum shifts to still higher f and disappears at $a_R = −1$ and $f \Rightarrow \infty$ while the minimum further deepens and also shifts to higher

f, approaching ≅1.65 for $a_R \Rightarrow -\infty$ (Fig. 3 c). Fixing $E_{P\text{-}P}$ instead of E_D produces similar behavior (Fig. 3 d), with $|\langle F \rangle|$ in the minimum and maximum equalizing for $a_R \cong -0.85$ when $f \cong 1.46$ and ≅5.97, respectively.

Similarly to the case of $f = 2$, the optimum $|\langle F \rangle|$ minimizes close to $a_R = -0.8$ (Fig. 4 a). Unlike at $f = 2$, the minimum is not null and thus permits some separation, but its height is only ~15% of $\langle F_3 \rangle_{max}$ at $a_R = 0$ and the resolution at a_R close to −0.8 would be poor. An analogous picture for fixed $E_{P\text{-}P}$ follows from Fig. 3 d. Then reducing $|a_R$ by use of *below-maximum* E_D/N or $E_{P\text{-}P}/N$ may be profitable, despite lower $(E/N)^3$ factors in eq (18). To optimize E_D and $F(t)$ simultaneously, we may combine eq (17) and eq (18) with either E_D or $E_{P\text{-}P}$ constraint into

$$d = K_0(0)(a_1^5 a_2^{-3} a_R^3)^{1/2} t_c \langle F \rangle \quad (20)$$

At any given a_R, the value of $|d|$ is greatest at the maxima of $|\langle F \rangle|$. For $f = 2$, that value grows with decreasing a_R up to $a_R \cong -0.48$, then drops to 0 at $a_R = -0.8$, and rises again (Fig. 4 b). In the result, the values of $|d|$ are lower for $-0.92 < a_R < -0.48$ than for $a_R = -0.48$. So $|d|$ can be increased by *decreasing* E_D/N until $a_R = -0.48$, which means reducing E_D by up to 28%. For optimum *f*, the minimum of $|d|$ becomes shallower and the sub-optimum region (S) shrinks to $-0.80 < a_R < -0.52$ (Fig. 4 b), but maximizing $|d|$ may still require decreasing E_D by up to 19%.

Hence, to maximize $|E_C|$, one should (Fig. 4 c): (i) for a_2 and a_1 with same signs, raise E_D/N to the allowed maximum while decreasing *f* from 2 to $f \cong 1.65 – 2.0$, depending on E_D/N; (ii) for a_2 and a_1 with opposite signs, raise E_D/N until a_R reaches −0.52 while increasing *f* from 2 to ≅2.6, then (if limitations on E_D/N permit) jump to $a_R = -0.8$ and $f = 1.24$ and raise E_D/N to the maximum while increasing *f* to ≅1.24 – 1.65, again depending on E_D/N. To enable all those capabilities, the value of *f* must be adjustable from 1.24 to 2.6. However, the fixed $f = 2$ provides $|E_C|$ within 7% of the maximum for $a_R > -0.52$ and other *f* have real worth only on the low-a_R side of region S (in the following, region L), especially $a_R \sim -(0.9 – 1.2)$ where $f_{opt} \cong 1.3$ grossly differs from 2 and $|E_C|$ at f_{opt} can reach 2.2× that at $f = 2$ (Fig. 4 c). Adopting $f = 2$ on the high-a_R side (region H) and $f = 1.35$ in region L provides $|E_C|$ within 9% of the maxima at any a_R (Fig. 4 c) while reducing the needed waveform flexibility to switching between two *f* values.

The present optimization may be extended to $a(E/N)$ including terms with $n > 2$ and/or waveforms constrained by $E_{P\text{-}P}$. With either constraint, the evolution of $\langle F_{2n+1} \rangle(f)$ dependences for $n > 2$ continues the trend from $n = 1$ to 2 (Fig. 3, Table 1). Hence the effect of adding a term with any $n > 2$ to the $n = 1$ term is akin to that of adding the $n = 2$ term considered here, but (for equal a_n/a_1 ratio) greater because the difference between $\langle F_{2n+1} \rangle$ and $\langle F_3 \rangle$ increases at higher *n* for any *f* value (Fig. 3 a, b). The addition of term(s) with $n > 2$ to the presently studied superposition of $n = 1$ and 2 terms may produce more complex dependences, which may be important at highest E/N values where the terms with $n > 2$ become substantial.

Relevance to Actual FAIMS Measurements

As the best waveforms of any class are determined by a_R, one may wonder what values are realistic. Of particular interest are the cases of $a_R \sim -(0.5 – 1.5)$ for which the optimum forms are most sensitive to a_R and notably differ from those for $a_R = 0$. The a_R for any ion/gas pair scales as $(E/N)2$ by eq (17), hence in theory one may reach any $|a_R|$ at strong enough fields and the notion of a "typical" a_R makes sense only for specific E_D/N magnitude. The original "full-size" FAIMS design largely adopted in Thermo Fisher systems features gap widths (*g*) of ~1.5 – 2.5 mm and operates at ambient pressure, normally employing E_D ~15 – 25 kV/cm or E_D/N ~60 – 100 Td: at weaker fields the drift nonlinearity rarely suffices for good separation

while the electrical breakdown threshold precludes much stronger fields (in N_2 or air).[53] That threshold increases for narrower gaps according to the Paschen's law,[53] and micromachined FAIMS devices (e.g., SDP-1 by Sionex with g = 0.5 mm)[7] allow E/N up to 140 Td. Same may be achieved by reducing the gas pressure, e.g., E/N = 180 Td was established at ~390 Torr.[49] The recent development of FAIMS "chips" with g ~10 μm by Owlstone has allowed raising E/N to ~400 Td.[48]

The value of a_R also depends on the ion(s) and gas through the a_2/a_1 ratio, and we shall now estimate those for global and targeted separations.

Global separations

In global analyses, one seeks to maximize the overall separation space, which in FAIMS means typical $|E_C|$ values as reviewed in the Introduction. For species with a_1 >0, typically a_2 <0 and a increases up to a maximum at certain E/N and decreases at greater E/N. This behavior (called "type B")[5] is ubiquitous for both atomic and polyatomic cations and anions with m < ~400 Da in N_2 or air at room temperature, including 13 of 17 protonated and 15 of 17 deprotonated amino acids,[54] protonated benzene and all 7 amines studied,[55] 8 protonated ketones up to decanone and 5 of their proton-bound dimers,[56] all 10 protonated organophosphorus compounds investigated and 7 of their dimers,[57] and I^- and anions of 5 common explosives and their degradants: 1,3-dinitrobenzene, 1,3,5-trinitrobenzene, p-mononitrotoluene, 2,4-dinitrotoluene, and 2,4,6-trinitrotoluene (TNT).[28] The magnitude of a_2/a_1 for those 72 species spans >3 orders of magnitude from $<10^{-6}$ to $>10^{-3}$ Td^{-2} (Fig. 5), but most values are on the order of $10^{-5} – 10^{-4}$ Td^{-2} regardless of the ion mass and the median a_2/a_1 is -5.5×10^{-5} Td^{-2}, for which $a_R = -0.5$ at E/N ~95 Td that is typical for either micromachined or "full-size" FAIMS. Exemplary species close to this median are $(Glu – H)^-$, $(TNT – H)^-$ (Table 2), and anions of other 4 explosive traces with $a_2/a_1 = -(5.2 – 6.0) \times 10^{-5}$ Td^{-2}. Half of the ions have higher $|a_2/a_1|$ values and $a_R = -0.5$ is reached at lower E/N; for some, e.g., H^+(Decanone) (Table 2), that occurs already at the lower end of practical FAIMS range (~60 – 70 Td). For most other ions, $|a_2/a_1| > 10^{-5}$ and a_R reaches −0.5 at E/N <220 Td, i.e., well within the range of Owlstone devices. Rarely, the a_2/a_1 values are so miniscule that a_R remains insignificant at E/N used in current FAIMS systems (Fig. 5). For example, for $(Ala – H)^-$ (Table 2), a_R would reach −0.5 only at E/N ~10^3 Td. As present a_1 and a_2 values were fit to FAIMS measurements at E_D/N ~70 – 120 Td, they cannot be used to accurately extrapolate $a(E/N)$ to much stronger fields where terms with higher n become important. Hence we compute a_R values at higher E_D/N not to maximize $|E_C|$ for specific ions, but to illustrate the E_D/N magnitude at which the optimum waveforms in typical scenarios materially deviate from those derived for $a_R = 0$.

The specific a_n and thus a_R at certain E_D for any ion depend on the gas composition, and $|a_2/a_1|$ values in some exceed those in N_2. For example, the humidity in ambient air (often used in field analyses) modifies $a(E)$. At any water vapor pressure tried[58] (P_w = 120 – 6000 ppm), ions of all 4 explosives and their degradants measured retain a_1 >0 and a_2 <0, but $|a_2/a_1|$ increases at higher P_w up to a maximum of 8.3×10^{-5} Td^{-2} that leads to a_R <−0.5 already at E_D = 80 Td.

For "type A" ions,[5] the $a(E/N)$ curves measured by FAIMS are fit by a_1 >0 and a_2 >0. In N_2 or air, this applies primarily to the smallest ions (e.g., Cl^-), but also some medium-size ones such as $(Pro – H)^-$ (Table 2). Though a_2/a_1 values can be quite high and produce substantial a_R even at low E_D/N (for Cl^-, a_R = 1.7 already at 70 Td), positive a_R hardly warrant waveform re-optimization, as discussed above. However, $a(E/N)$ functions cannot increase indefinitely: at $E/N \Rightarrow \infty$, the ion/molecule potential always approaches the hard-shell limit where K drops[32] at higher E/N. Thus, when a_1 >0, the value of a maximizes at finite E/N (exhibiting type B behavior) and observation of type A ions is a mere artifact of limited E/N range sampled in FAIMS. (Most type A ions are small because the maxima of K shift to greater E/N for deeper

ion/molecule potentials that are more common to smaller and particularly atomic ions where the gas molecule can come close to the charged site.) That type A ions inevitably convert to type B at higher E/N implies that $a_n < 0$ for some $n > 1$. Though that n may equal 3 or greater, the effect on optimum waveform at E/N near or above the maximum K will overall resemble that explored here for type B behavior due to $a_2 < 0$.

Targeted separations

As a filtering technique, FAIMS (like quadrupole MS) is mainly useful for targeted analyses, where removal of other species does no harm. In quadrupole MS, the conditions for maximum resolution of targeted analyses (in the selected ion monitoring mode) and global analyses (in the scanning mode) are identical. That is not quite true in FAIMS.

Targeted separations depend on the *spread* between d and thus E_C values of two or more species and not E_C of a single ion, as indicated by eq (9). To optimize $E(t)$ for resolution of analytes X and Y, we should replace the coefficients a_n for one ion by $(a_{n,X} - a_{n,Y})$. Then the dependences of optimum waveforms on a_R found above continue to apply, with a_R still given by eq (17) but a_2/a_1 defined as:

$$a_2/a_1=(a_{2,X} - a_{2,Y})/(a_{1,X} - a_{1,Y}) \quad (21)$$

A prototypical isomeric separation in biological analyses is that of leucine and isoleucine amino acids. Those were resolved by FAIMS as deprotonated anions[59] in N_2 and protonated cations[4] in 1:1 He/N_2, in both cases just barely. For anions, the experimental E_D/N was 67 Td where a_R equals −0.15 for $(Leu - H)^-$ and −0.05 for $(Ile - H)^-$ (Table 2). Both values suggest that the best $F(t)$ for this separation is essentially identical to that for $a_2 = 0$. However, the difference between $a(E/N)$ of Ile and Leu anions has $\{a_1 = 0.28 \times 10^{-6}$ Td^{-2}; $a_2 = -1.27 \times 10^{-10}$ Td$^{-4}\}$, leading to very high $|a_2/a_1| = 45 \times 10^{-5}$ Td^{-2} and $a_R = -2.0$ at same 67 Td. Hence this separation can likely be improved using the waveforms optimized for region L.

This situation is not limited to isomers. For the deprotonated hydroxyproline (ProOH) (Table 2) that is isobaric to $(Leu - H)^-$, the value of a_R at 67 Td equals −0.01, and the optimum $E(t)$ is determined solely by the $n = 1$ term. However, the differential $a(E/N)$ of $(ProOH - H)^-$ and $(Leu - H)^-$ has $\{a_1 = 0.12 \times 10^{-6}$ Td^{-2}; $a_2 = 1.77 \times 10^{-10}$ Td$^{-4}\}$, and a_2/a_1 is an extreme $\sim 150 \times 10^{-5}$ Td^{-2} leading to $a_R = 6.6$. So, even at this low E_D/N, the optimum $F(t)$ is determined almost only by the $n > 1$ terms. That is of little consequence here because $a_R > 0$, but isobars with similarly large negative a_2/a_1 certainly exist.

Much greater magnitude of a_2/a_1 by eq (21) compared to a_2/a_1 for either X or Y in above cases reflects[44] a lower correlation of a_2 values for different ions compared to that of a_1. Opposite examples exist: the differential $a(E/N)$ of $(Ser - H)^-$ and $(Leu - H)^-$ has $\{a_1 = 6.97 \times 10^{-6}$ Td^{-2}; $a_2 = 0.08 \times 10^{-10}$ Td$^{-4}\}$, and $a_2/a_1 = 0.11 \times 10^{-5}$ Td^{-2} is much lower than the values for either species (Table 2). However, the median values of $|a_2/a_1|$ (in 10^{-5} Td^{-2}) for 17 amino acids studied[54] and their 136 possible pairs are, respectively, 1.9 vs. 4.7 for cations and 1.7 vs. 5.6 for anions. The results for subsets of ions and pairs with $a_2/a_1 < 0$ are similar: the medians are 1.9 vs. 4.6 for cations and 2.1 vs. 7.9 for anions. That is, statistically the mean effective $|a_R|$ values for pairs of amino acid ions at any E/N are ~3× those for individual ions and $a_R \sim -0.5$ for pairs with $a_2/a_1 < 0$ will be reached at E/N lower by a factor of $\sim\sqrt{3}$: on average ~90 Td typical in standard FAIMS systems vs. ~160 Td used at reduced pressure or in miniature chips. Thus, the distinction between optimum waveforms at $a_R = 0$ and ~−1 is likely more important in targeted analyses.

Conclusions

The asymmetric waveforms $E(t)$ that maximize resolving power (R) of FAIMS materially depend on the $a(E/N)$ profile(s) for ion(s) of interest. The optimum $E(t)$ is defined by E/N and ratios of coefficients a_n with the terms of $a(E/N)$ expansion in a power series: truncating to two terms, the key quantity is $a_R = a_2(E/N)^2/a_1$. For positive a_R (when the terms add), the effect is small: $E(t)$ optimized without considering the $a(E/N)$ profile (i.e., for $a_R = 0$) provide R within ~7% of the maximum. In this case, one should always maximize the $E(t)$ amplitude, E_D, within the power supply or electrical breakdown constraints. With negative a_R, the 2nd term is subtracted from the 1st and, at $a_R \sim -1$, the difference that underlies FAIMS separation is not close to either. This produces "sub-optimum" (S) regions at a_R within the $-(0.5 – 0.9)$ range, where separation is improved via *reducing* E_D by up to ~20 – 30% from the maximum until $|a_R|$ decreases to the region boundary. The optimum $E(t)$ remain close to those at $a_R = 0$ in regions H on the high-a_R side of S, but substantially differ in regions L on the low-a_R side, where using the $E(t)$ optimized at $a_R = 0$ reduces R for all three classes by up to 2.2 times. In L, the optimum $E(t)$ also depends on a_R, but >90% of maximum R can always be achieved using fixed forms intermediate between those optimum on the L/S boundary and for $a_R \Rightarrow \infty$. Thus re-optimization of $E(t)$ for each a_R can in practice be emulated by selecting one of the two forms (Fig. 6). In H, we can use $E(t)$ optimized for $a_R = 0$ and employed in present FAIMS systems, while the new $E(t)$ found here can produce significant gains in L. Though we included only the first two terms of the $a(E/N)$ expansion, the optimum waveforms are primarily dictated by (constructive or destructive) interference of terms, and not their specific powers. Hence, addition of further terms (which are often quite significant in advanced FAIMS designs using E/N >100 Td) will produce similar effects that can be treated using the present framework.

Ions in FAIMS have been grouped into type A where the $a(E/N)$ function increases, B where it has a maximum, and C where it decreases.[5] Analyses of type A and C ions fall into the H region, and new waveforms proposed here for the L region would be used for type B species that include most ions of explosives in air or N_2 over a broad range of humidity. However, all type A ions convert to type B at higher E/N values, and thus new waveforms become relevant for species deemed type A as new miniaturized or reduced-pressure FAIMS systems using higher E/N are introduced. The key applications of FAIMS are to targeted analyses that are based not on individual $a(E/N)$ functions but on their spread that can behave as "type B" even when neither ion does. Hence new waveforms intended for L region may improve resolution of specific ions despite R for each maximized by existing $E(t)$.

Though presently optimized waveforms maximize FAIMS specificity for an ion or ion pair, different $E(t)$ may be desired for other reasons. In particular, a $F(t)$ that sort ions by a_n values for n >1 without regard to a_1 may enable higher-order differential (HOD) IMS[44] analyses that should be substantially orthogonal to FAIMS based on whole $a(E/N)$. As optimum $E(t)$ for separation of ion pairs depend on their differential a_n values, the best forms for resolution of three or more ions will generally deviate from those for each pairwise combination; their optimization remains to be explored. In contrast, absolute ion mobilities that underlie conventional IMS depend on E weakly or not at all within the measurement accuracy, and ions with equal K at some E are unlikely to be resolved at any practical E. The possibility to tailor analyses by modifying $F(t)$ is one manifestation of the unique flexibility of differential IMS.

Acknowledgements

We thank Drs. Keqi Tang, Aleksey Tolmachev, and Robert Ewing (PNNL) for discussions of optimization and analytical use of FAIMS. This research has been supported by PNNL Initiative for Explosives Detection and NIH National Center for Research Resources (RR 18522) located in the Environmental Molecular Sciences Laboratory, a national scientific user facility at PNNL sponsored by the U.S. Department of Energy Office of Biological and Environmental Research. PNNL is operated for the DOE by Battelle under Contract DE-AC05-76RLO 1830.

References

1. Buryakov IA, Krylov EV, Nazarov EG, Rasulev UK. A New Method of Separation of Multi-Atomic Ions by Mobility at Atmospheric Pressure Using a High-Frequency Amplitude-Asymmetric Strong Electric Field. Int. J. Mass Spectrom. Ion Proc 1993;128:143–148.
2. Purves RW, Guevremont R. Electrospray Ionization High-Field Asymmetric Waveform Ion Mobility Spectrometry - Mass Spectrometry. Anal. Chem 1999;71:2346–2357.
3. Miller RA, Eiceman GA, Nazarov EG, King AT. A Novel Micromachined High-Field Asymmetric Waveform-Ion Mobility Spectrometer. Sens. Actuat. B 2000;67:300–306.
4. Shvartsburg AA, Li F, Tang K, Smith RD. High-Resolution Field Asymmetric Waveform Ion Mobility Spectrometry Using New Planar Geometry Analyzers. Anal. Chem 2006;78:3706–3714. [PubMed: 16737227]
5. Guevremont R. High-Field Asymmetric Waveform Ion Mobility Spectrometry: A New Tool for Mass Spectrometry. J. Chromatogr. A 2004;1058:3–19. [PubMed: 15595648]
6. Gabryelski W, Froese KL. Characterization of Naphthenic Acids by Electrospray Ionization High-Field Asymmetric Waveform Ion Mobility Spectrometry Mass Spectrometry. Anal. Chem 2003;75:4612–4623. [PubMed: 14632072]
7. Eiceman GA, Krylov EV, Tadjikov B, Ewing RG, Nazarov EG, Miller RA. Differential Mobility Spectrometry of Chlorocarbons with a Micro-Fabricated Drift Tube. Analyst 2004;129:297–304. [PubMed: 15042159]
8. Gabryelski W, Wu F, Froese KL. Comparison of High-Field Asymmetric Waveform Ion Mobility Spectrometry with GC Methods in Analysis of Haloacetic Acids in Drinking Water. Anal. Chem 2003;75:2478–2486. [PubMed: 12918993]
9. Sander LC, Sharpless KE, Satterfield MB, Ihara T, Phinney KW, Yen JH, Wise SA, Gay ML, Lam JW, McCooeye M, Gardner G, Fraser C, Sturgeon R, Roman M. Determination of Ephedrine Alkaloids in Dietary Supplement Standard Reference Materials. Anal. Chem 2005;77:3101–3112. [PubMed: 15889898]
10. Liu X, Zhao YY, Chan K, Hrudey SE, Li XF, Li JJ. Analysis of Nitrosamines by Capillary Electrospray-High-Field Asymmetric Waveform Ion Mobility Spectrometry-MS with Programmed Compensation Voltage. Electrophoresis 2007;28:1327–1334. [PubMed: 17367110]
11. Schmidt H, Tadjimukhamedov F, Mohrenz IV, Smith GB, Eiceman GA. Microfabricated Differential Mobility Spectrometry with Pyrolysis Gas Chromatography for Chemical Characterization of Bacteria. Anal. Chem 2004;76:5208–5217. [PubMed: 15373463]
12. Shnayderman M, Mansfield B, Yip P, Clark HA, Krebs MD, Cohen SJ, Zeskind JE, Ryan ET, Dorkin HL, Callahan MV, Stair TO, Gelfand JA, Gill CJ, Hitt B, Davis CE. Species-Specific Bacterial Identification Using Differential Mobility Spectrometry and Bioinformatics Pattern Recognition. Anal. Chem 2005;77:5930–5937. [PubMed: 16159124]
13. Lu Y, Harrington PB. Forensic Applications of Gas Chromatography-Differential Mobility Spectrometry with Two-Way Classification of Ignitable Liquids from Fire Debris. Anal. Chem 2007;79:6752–6759. [PubMed: 17683164]
14. Guevremont R, Barnett DA, Purves RW, Vandermey J. Analysis of a Tryptic Digest of Pig Hemoglobin Using ESI-FAIMS-MS. Anal. Chem 2000;72:4577–4584. [PubMed: 11028613]
15. Venne K, Bonneil E, Eng K, Thibault P. Improvement in Peptide Detection for Proteomics Analyses Using NanoLC-MS and High-Field Asymmetry Waveform Ion Mobility Mass Spectrometry. Anal. Chem 2005;77:2176–2186. [PubMed: 15801752]
16. Tang K, Li F, Shvartsburg AA, Strittmatter EF, Smith RD. Two-Dimensional Gas-Phase Separations Coupled to Mass Spectrometry for Analysis of Complex Mixtures. Anal. Chem 2005;77:6381–6388. [PubMed: 16194103]
17. Li J, Purves RW, Richards JC. Coupling Capillary Electrophoresis and High-Field Asymmetric Waveform Ion Mobility Spectrometry-Mass Spectrometry for the Analysis of Complex Lipopolysaccharides. Anal. Chem 2004;76:4676–4683. [PubMed: 15307776]
18. Kapron J, Wu J, Mauriala T, Clark P, Purves RW, Bateman KP. Simultaneous Analysis of Prostanoids Using Liquid Chromatography/High-Field Asymmetric Waveform Ion Mobility Spectrometry/

Tandem Mass Spectrometry. Rapid Commun. Mass Spectrom 2006;20:1504–1510. [PubMed: 16628569]

19. Hatsis P, Brockman AH, Wu JT. Evaluation of High-Field Asymmetric Waveform Ion Mobility Spectrometry Coupled to Nanoelectrospray Ionization for Bioanalysis in Drug Discovery. Rapid Commun. Mass Spectrom 2007;21:2295–2300. [PubMed: 17577878]
20. Mie A, Jornten-Karlsson M, Axelsson BO, Ray A, Reimann CT. Enantiomer Separation of Amino Acids by Complexation with Chiral Reference Compounds and High-Field Asymmetric Waveform Ion Mobility Spectrometry: Preliminary Results and Possible Limitations. Anal. Chem 2007;79:2850–2858. [PubMed: 17326611]
21. Purves RW, Barnett DA, Ells B, Guevremont R. Elongated Conformers of Charge States +11 to +15 of Bovine Ubiquitin Studied Using ESI-FAIMS-MS. J. Am. Soc. Mass Spectrom 2001;12:894–901. [PubMed: 11506222]
22. Borysik AJH, Read P, Little DR, Bateman RH, Radford SE, Ashcroft AE. Separation of β_2-microglobulin Conformers by High-Field Asymmetric Waveform Ion Mobility Spectrometry (FAIMS) Coupled to Electrospray Ionisation Mass Spectrometry. Rapid Commun. Mass Spectrom 2004;18:2229–2234. [PubMed: 15384141]
23. Robinson EW, Leib RD, Willams ER. The Role of Conformation on Electron Capture Dissociation of Ubiquitin. J. Am. Soc. Mass Spectrom 2006;17:1470–1480.
24. Shvartsburg AA, Bryskiewicz T, Purves RW, Tang K, Guevremont R, Smith RD. Field Asymmetric Waveform Ion Mobility Spectrometry Studies of Proteins: Dipole Alignment in Ion Mobility Spectrometry? J. Phys. Chem. B 2006;110:21966–21980. [PubMed: 17064166]
25. Shvartsburg AA, Li F, Tang K, Smith RD. Characterizing the Structures and Folding of Free Proteins Using 2-D Gas-Phase Separations: Observation of Multiple Unfolded Conformers. Anal. Chem 2006;78:3304–3315. [PubMed: 16689531]ibid 8575.
26. Buryakov IA, Kolomiets YN, Luppu BV. Detection of Explosive Vapors in the Air Using an Ion Drift Nonlinearity Spectrometer. J. Anal. Chem 2001;56:336–340.
27. Buryakov IA, Kolomiets YN. Rapid Determination of Explosives and Narcotics Using a Multicapillary-Column Gas Chromatograph and an Ion-Mobility Spectrometer. J. Anal. Chem 2003;58:944–950.
28. Buryakov IA. Qualitative Analysis of Trace Constituents by Ion Mobility Increment Spectrometer. Talanta 2003;61:369–375. [PubMed: 18969196]
29. Buryakov IA. Express Analysis of Explosives, Chemical Warfare Agents and Drugs with Multicapillary Column Gas Chromatography and Ion Mobility Increment Spectrometry. J. Chromatogr. B 2004;800:75–82.
30. Eiceman GA, Krylov E, Krylova N, Nazarov EG, Miller RA. Separation of Ions from Explosives in Differential Mobility Spectrometry by Vapor-Modified Drift Gas. Anal. Chem 2004;76:4937–4944. [PubMed: 15373426]
31. Buryakov IA, Kolomietz YN, Bolotov AV, Vasin AI, Vlasov YN. Registration of Lewisite Vapors in Air Using an Ion Mobility Spectrometer. J. Anal. Chem 2002;57:606–610.
32. McDaniel, EW.; Mason, EA. Transport Properties of Ions in Gases. NY: Wiley; 1988.
33. Krylov EV, Nazarov EG, Miller RA. Differential Mobility Spectrometer: Model of Operation. Int. J. Mass Spectrom 2007;266:76–85.
34. Eiceman, GA.; Karpas, Z. Ion Mobility Spectrometry. Boca Raton, FL: CRC; 2005.
35. Akridge GR, Ellis HW, Pai RY, McDaniel EW. Mobilities of Li^+ Ions in He, Ne, and Ar and of Na^+ ions in He, Ne, Ar, and CO_2. J. Chem. Phys 1975;62:4578–4579.
36. Iinuma K, Imai M, Satoh Y, Takebe M. Mobilities of Li^+ Ions in HCl, HBr, and HI at Room Temperature. J. Chem. Phys 1988;89:7035–7036.
37. Barnett DA, Ells B, Guevremont R, Purves RW, Viehland LA. Evaluation of Carrier Gases for Use in High-Field Asymmetric Waveform Ion Mobility Spectrometry. J. Am. Soc. Mass Spectrom 2000;11:1125–1133. [PubMed: 11118120]
38. Ruotolo BT, McLean JA, Gillig KJ, Russell DH. The Influence and Utility of Varying Field Strength for the Separation of Tryptic Peptides by Ion Mobility-Mass Spectrometry. J. Am. Soc. Mass Spectrom 2005;16:158–165. [PubMed: 15694766]

39. Gorshkov MA. Method for Analysis of Additives to Gases. 1982USSR Inventor's Certificate # 966,583
40. Buryakov IA, Krylov EV, Soldatov VP. Method for Analysis of Additives to Gases. 1987USSR Inventor's Certificate # 1,337,934
41. Buryakov IA, Krylov EV, Makas AL, Nazarov EG, Pervukhin VV, Rasulev UK. Ion Division by their Mobility in High-Tension Alternating Electric Field. Tech. Phys. Lett 1991;17:412.
42. Krylov EV. Comparison of the Planar and Coaxial Field Asymmetrical Waveform Ion Mobility Spectrometer. Int. J. Mass Spectrom 2003;225:39–51.
43. Elistratov AA, Shibkov SV. A Model of Nonlinear Ion Drift Spectrometry for Gas Detectors with Separating Chamber of Cylindrical Geometry. Tech. Phys. Lett 2004;30:183–185.
44. Shvartsburg AA, Mashkevich SV, Smith RD. Feasibility of Higher-Order Differential Ion Mobility Separations Using New Asymmetric Waveforms. J. Phys. Chem. A 2006;110:2663–2673. [PubMed: 16494377]
45. Krylov EV. Pulses of Special Shapes Formed on a Capacitive Load. Inst. Exp. Tech 1997;40:628–631.
46. Shvartsburg AA, Tang K, Smith RD. Optimization of the Design and Operation of FAIMS Analyzers. J. Am. Soc. Mass Spectrom 2005;16:2–12. [PubMed: 15653358]
47. Shvartsburg AA, Tang K, Smith RD. Modeling the Resolution and Sensitivity of FAIMS Analyses. J. Am. Soc. Mass Spectrom 2004;15:1487–1498. [PubMed: 15465362]
48. Boyle, B.; Koehl, A.; Parris, R.; Ruiz-Alonso, D.; Rush, M.; Wilks, A. A MEMS Fabricated Device for Field Asymmetric Ion Mobility Spectrometry. New Orleans, LA. Proceedings of the Pittcon 2008 Conference;
49. Nazarov EG, Coy SL, Krylov EV, Miller RA, Eiceman GA. Pressure Effects in Differential Mobility Spectrometry. Anal. Chem 2006;78:7697–7706. [PubMed: 17105161]
50. Papanastasiou D, Wollnik H, Rico G, Tadjimukhamedov F, Mueller W, Eiceman GA. Differential Mobility Separation of Ions Using a Rectangular Asymmetric Waveform. J. Phys. Chem. A 2008;112:3638–3645. [PubMed: 18338877]
51. Buryakov IA, Krylov EV, Soldatov VP. Drift Spectrometer for Trace Detection of Substances in Gases. 1989USSR Inventor's Certificate # 1,412,447
52. Viehland LA, Guevremont R, Purves RW, Barnett DA. Comparison of High-Field Ion Mobility Obtained from Drift Tubes and a FAIMS Apparatus. Int. J. Mass Spectrom 2000;197:123–130.
53. Meek JM, Craggs JD. Electrical Breakdown of Gases. 1978
54. Guevremont R, Barnett DA, Purves RW, Viehland LA. Calculation of Ion Mobilities from Electrospray Ionization High-Field Asymmetric Waveform Ion Mobility Spectrometry Mass Spectrometry. J. Chem. Phys 2001;114:10270–10277.
55. Buryakov IA. Determination of Kinetic Transport Coefficients for Ions in Air as Functions of Electric Field and Temperature. Tech. Phys 2004;49:967–972.
56. Krylov E, Nazarov EG, Miller RA, Tadjikov B, Eiceman GA. Field Dependence of Mobilities for Gas-Phase-Protonated Monomers and Proton-Bound Dimers of Ketones by Planar Field Asymmetric Waveform Ion Mobility Spectrometer (PFAIMS). J. Phys. Chem. A 2002;106:5437–5444. [PubMed: 12132535]
57. Krylova N, Krylov E, Eiceman GA, Stone JA. Effect of Moisture on the Field Dependence of Mobility for Gas-Phase Ions of Organophosphorus Compounds at Atmospheric Pressure with Field Asymmetric Ion Mobility Spectrometry. J. Phys. Chem. A 2003;107:3648–3654. [PubMed: 12830828]
58. Buryakov IA. Effect of the Water Vapor Density on the Field Dependence of the Ion Mobility Increment for Nitro Compounds in Air. Tech. Phys. Lett 2007;33:861–864.
59. Barnett DA, Ells B, Guevremont R, Purves RW. Separation of Leucine and Isoleucine by Electrospray Ionization High-Field Asymmetric Waveform Ion Mobility Spectrometry - Mass Spectrometry. J. Am. Soc. Mass Spectrom 1999;10:1279–1284.

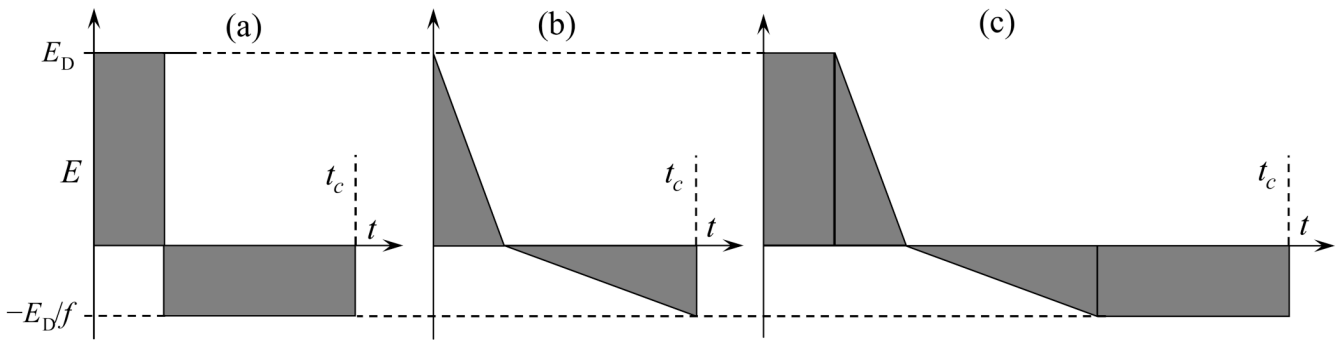

Fig. 1.
Asymmetric waveforms: rectangular (a), triangular (b), and trapezoidal (c).

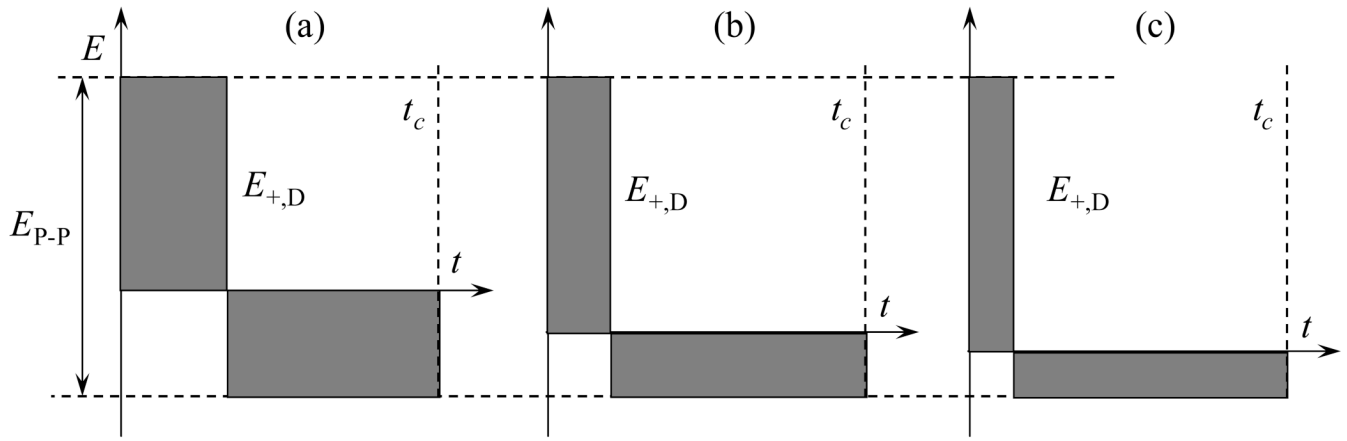

Fig. 2.
Rectangular waveforms with fixed peak-to-peak amplitude have greater peak amplitudes at higher *f*: profiles with *f* = 2 (a), 4 (b), and 6 (c).

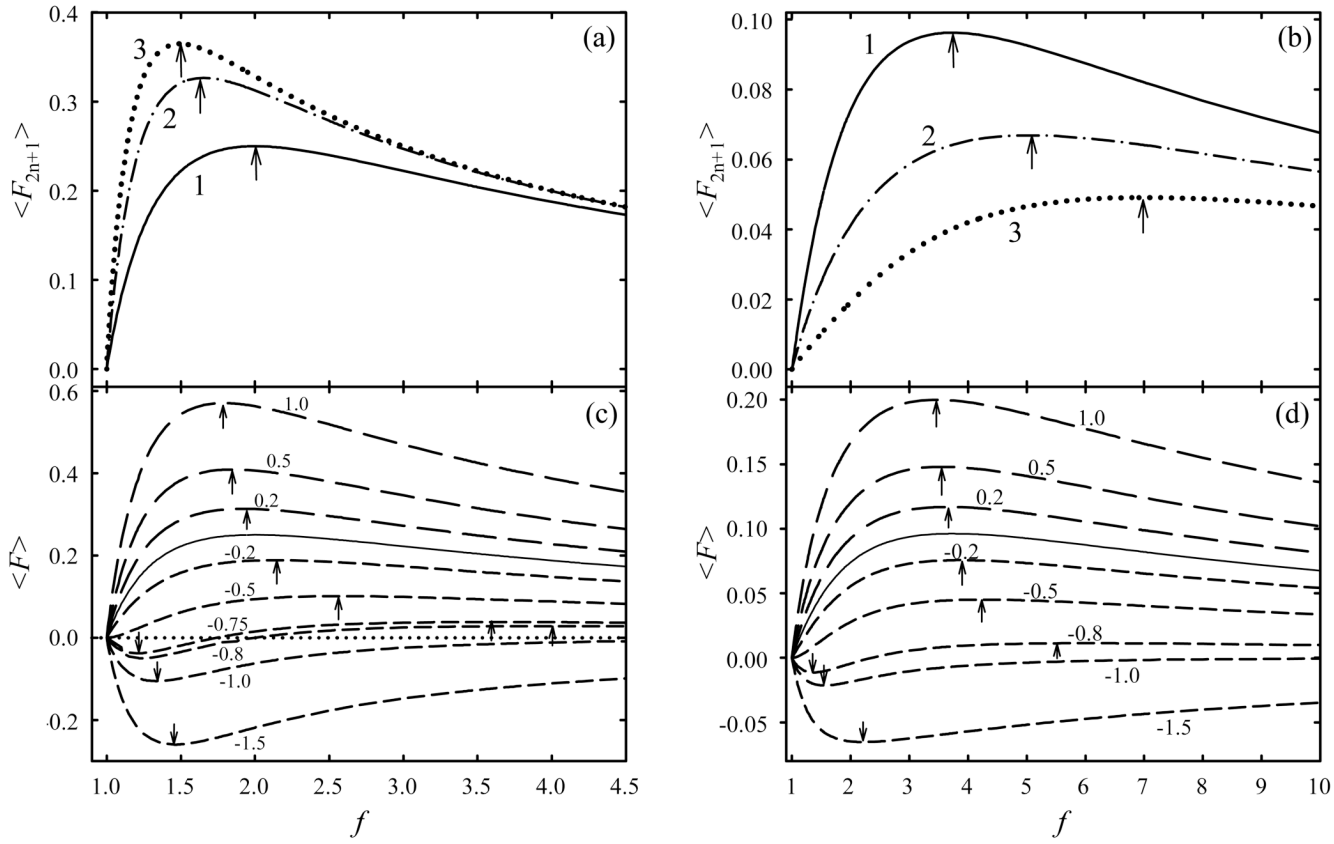

Fig. 3.

Form-factors of rectangular $E(t)$ constrained by E_D (a, c) and $E_{p\text{-}p}$ (b, d) for hypothetical ions with various a_n values. In (a, b), $a_n = 1$ for $n = 1 – 3$ as labeled and $a_n = 0$ for other n. In (c, d), $a_n = 0$ for $n > 2$ and a_R values are labeled, curves are for $a_R = 0$ (solid line), $a_R > 0$ (long dash), and $a_R < 0$ (short dash). The maxima are marked by arrows up, minima by arrows down. The dotted line in (c) is for $\langle F \rangle = 0$ (no separation).

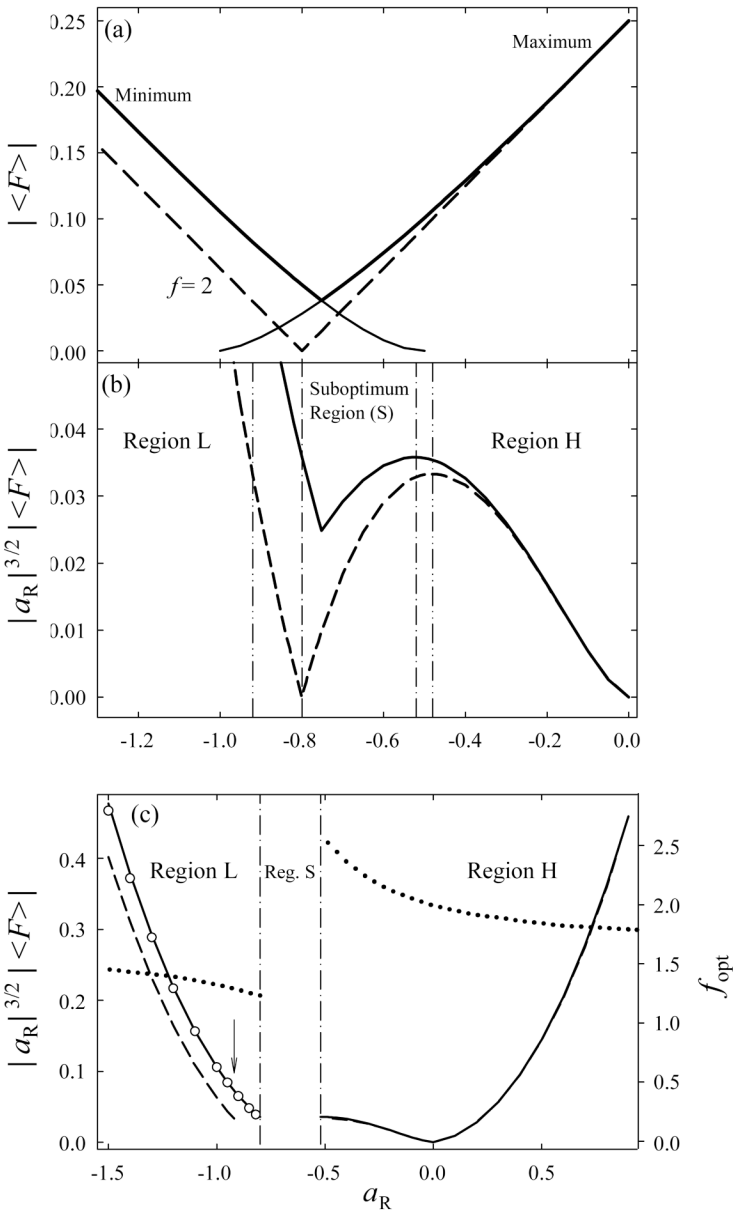

Fig. 4.

Properties of separations using rectangular $E(t)$ with E_D constraint: (a) absolute form-factor (derived from Fig. 3 c) and (b, c - left axis) absolute ion displacements per FAIMS cycle [in the units of $a_1^{5/2}a_2^{-3/2}K_0(0)t_c$] for fixed (b) and variable (c) E_D. Thin solid lines (a) are for maximum or minimum $\langle F \rangle$ as labeled, thick solid lines are for maximum $|\langle F \rangle|$, dashed lines are for fixed f as marked, and circles (c, region L) are for $f = 1.35$. Vertical lines show the region boundaries: dash-dot-dot (b) for fixed f and dash-dot (b, c) for variable f. In (c), the arrow points to the greatest difference between $|d|$ with optimum f and $f = 2$ (that is best at $a_R = 0$) and the dotted line shows optimum f (right axis).

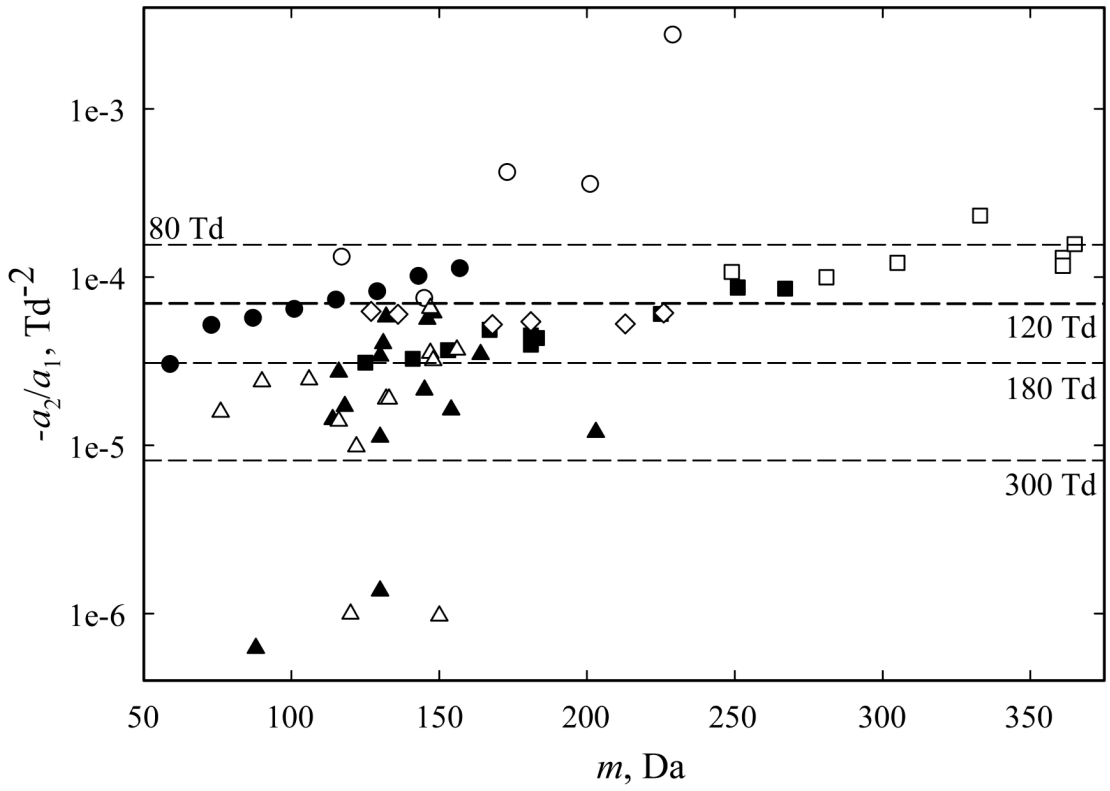

Fig. 5.

Measured values of a_2/a_1 for representative type B ions: protonated (Δ) and deprotonated (▲) amino acids,[54] protonated benzene and amines (▼), protonated ketone monomers (●) and dimers (○),[56] protonated monomers (■) and dimers (□) of organophosporus compounds,[57] and deprotonated or radical anions of explosives[28] (◊).

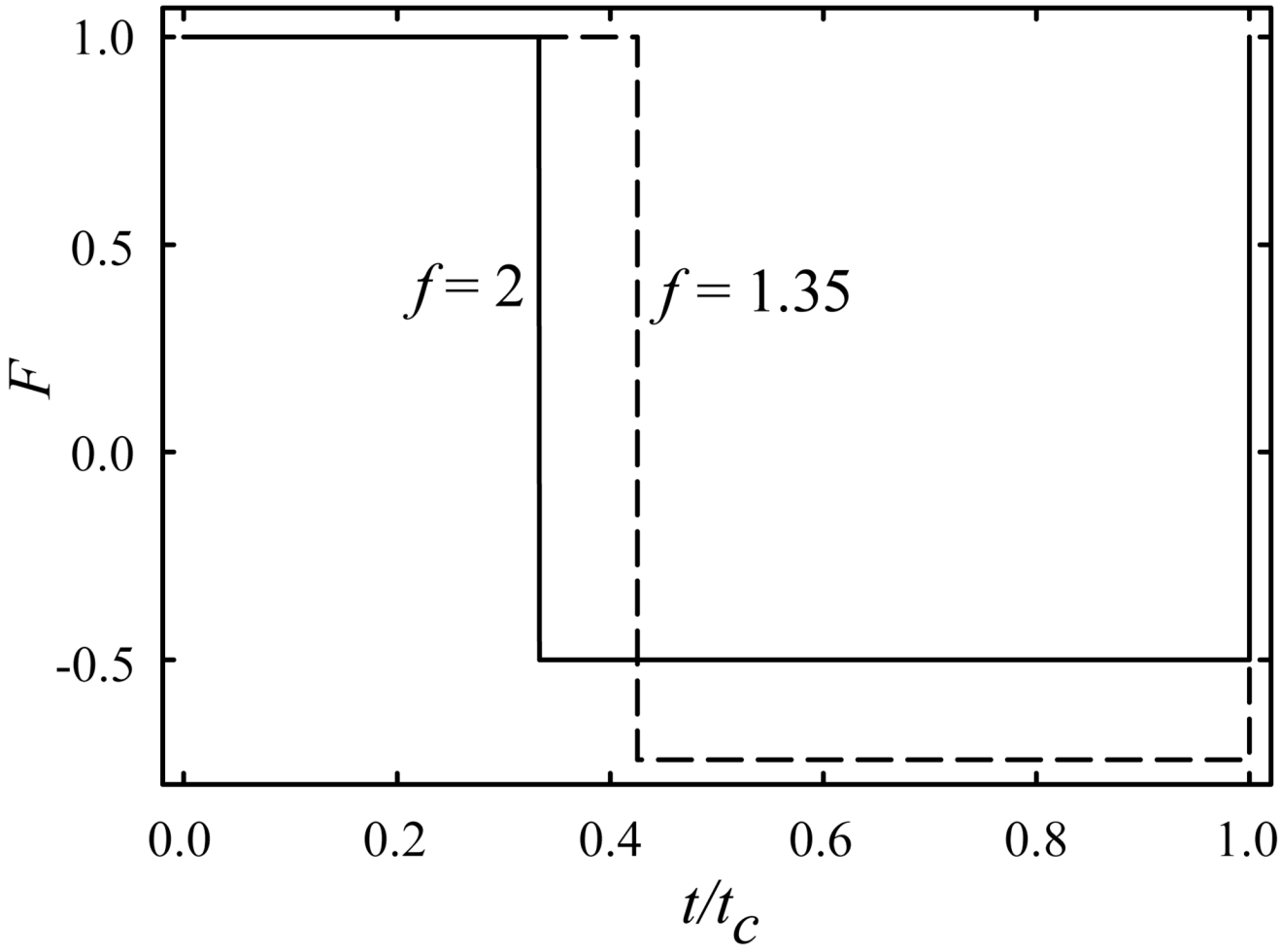

Fig. 6.
Near-optimum waveforms proposed for use in H and L regions, values of *f* are marked.

Table 1

Optimum f and maximum m $\langle F_{2n+1} \rangle$ F values up to $n = 5$ for rectangular $F(t)$.

Separation order	Rectangular (E_D fixed)		Rectangular ($E_{P\text{-}P}$ fixed)	
	f_{opt}	$\langle F_n \rangle$	f_{opt}	$\langle F_n \rangle$
$n = 1$	2	0.250	3.73	0.0962
$n = 2$	1.65	0.326	5.04	0.0669
$n = 3$	1.49	0.365	7.00	0.0491
$n = 4$	1.40	0.388	9.00	0.0387
$n = 5$	1.34	0.404	11.0	0.0320

Table 2

Values of a_1 and a_2 for some ions in air or N_2 (at T = 300 K) measured using FAIMS.[a]

Species	Cl^-	Ala	Pro	Ser	Leu	Ile	ProOH	Glu	H^+(Dec.)	TNT
Mass, Da	35	88	114	104	130	130	130	146	157	226
a_1, 10^{-6} Td^{-2}	18.7	12.0	7.82	12.4	5.43	5.15	5.55	7.12	4.6	4.4
a_2, 10^{-10} Td^{-4}	64	−0.075	0.50	-1.77	−1.85	−0.58	−0.08	−4.0	−5.2	−2.7
a_2/a_1, 10^{-5} Td^{-2}	34	−0.063	0.64	−1.4	−3.4	−1.1	−0.14	−5.6	−11.3	−6.1

[a] Data are from [47, 52] for Cl^-, [54] for deprotonated amino acids (alanine, proline, serine, leucine, isoleucine, hydroxyproline, and glutamic acid), [56] for H^+(Decanone), and [28] for the deprotonated TNT.